Letter

Extreme Sound Confinement From Quasibound States in the Continuum

Sibo Huang,[1] Tuo Liu,[2,3] Zhiling Zhou,[1] Xu Wang,[1,*] Jie Zhu,[2,3,†] and Yong Li[1,‡]

[1] *Institute of Acoustics, Tongji University, Shanghai 200092, People's Republic of China*

[2] *The Hong Kong Polytechnic University Shenzhen Research Institute, Shenzhen 518057, People's Republic of China*

[3] *Department of Mechanical Engineering, The Hong Kong Polytechnic University, Hung Hom, Kowloon, Hong Kong SAR, People's Republic of China*

(Received 12 November 2019; revised 1 July 2020; accepted 6 July 2020; published 7 August 2020)

Extreme confinement of incident acoustic waves remains challenging due to the conflict between reflection elimination and weak dissipation. In this study, by realizing a Friedrich-Wintgen quasibound state in the continuum (quasi-BIC), we demonstrate that sound confinement with an arbitrarily high quality factor becomes possible. The proposed proof-of-concept system consists of two slightly detuned resonators sharing a single-port radiating channel and supports a quasi-BIC. When operating with balanced low radiative and dissipative decay rates, it allows frequency-selective trapping of the incoming sound waves. The effect is experimentally and numerically validated as evidenced by the observation of an ultranarrow reflection dip (zero reflection at 420.8 Hz) along with intensive field enhancement (24.5 dB). We also show that the quality factor can be further improved by simultaneously reducing the detuning and the intrinsic loss. Our work breaks through the barrier in obtaining extreme sound confinement and may offer opportunities for the development of acoustic sensors, filters, and harvesters.

DOI: 10.1103/PhysRevApplied.14.021001

a. Introduction. Bound states in the continuum (BICs) are peculiar states perfectly confined with no radiation yet lie inside a continuous spectrum of radiating waves [1,2]. BICs were originally proposed in quantum mechanics [1], and then shown to occur in many classical physics systems [3–26]. Distinct from the conventional bound states locating outside the continuum, BICs can be regarded as resonance with zero leakage and zero linewidth (infinitely high quality factor, Q) residing inside the continuum [2]. In optics and photonics, many high-efficient practical applications have been presented by constructing quasi-BICs, such as lasers [19–22], sensors [23,24], and filters [25,26].

For acoustic systems, the ultrahigh Q factor and extremely low radiation of quasi-BICs suggest a pathway to the realization of long-lifetime sound confinement. Acoustic BICs, also referred to as embedded trapped modes, were first observed during the study of pressure enhancement near a cascade of parallel plates in a wind tunnel [2,3,27,28]. Those "plate-in-waveguide" systems have reflection symmetry, so that symmetry-protected BICs can be excited by waves inside the systems (such as excited by vortex shedding from the trailing edges of plates aligned with the flow) [29–35]. However, those BIC-supporting systems are incapable of confining incoming waves from the outside. Another type of acoustic BIC-supporting system was investigated in the hypothetical lossless systems of waveguides with side-branched cavities [4–7]. When the resonance frequencies of the side-branched Fabry-Perot cavities (placed far away from each other) or the spacing between them is tuned to make the round-trip phase shifts add up to an integer multiple of 2π, the Fabry-Perot BICs are formed [4,5]. Besides, for two resonators at the same location, a Friedrich-Wintgen BIC can be constructed by modulating their radiations to achieve a destructive interference [6,7]. So far, those BIC-supporting systems have never been experimentally witnessed [4].

In this study, we present an acoustic Friedrich-Wintgen quasi-BIC-supporting system allowing strong confinement of incoming waves. The system features a very low radiative decay rate that compensates an identically low dissipative decay rate to completely trap the incoming waves. Consequently, the trapped waves are able to survive the low dissipative decay rate for a long time, leading to a long-lifetime extreme sound confinement. The experimental and simulation results validate the trapping effect and the intensive sound-field enhancement. It is also demonstrated that in the case of smaller radiative and dissipative decay rates guaranteed by a correspondingly larger structure, the sound-confinement lifetime can be further prolonged.

*xuwang@tongji.edu.cn
†jiezhu@polyu.edu.hk
‡yongli@tongji.edu.cn

b. Concept of the acoustic Friedrich-Wintgen quasi-BIC. We take a pair of detuned resonant cavities as a proof-of-concept demonstration. First, for incident acoustic waves impinging into a lossless resonant cavity, sound confinement is impossible due to total reflection [Fig. 1(a)]. Introducing intrinsic (thermal-viscous) loss to the cavity can reduce the reflection and even achieve a so-called perfect absorber [36–43] [Fig. 1(b)]. However, it requires a considerable loss of the structure to form such a reflection elimination. Consequently, the incoming sound waves are quickly dissipated rather than confined in the system. Therefore, extreme confinement of incident waves occurs only when a zero reflection and an ultralow dissipation are simultaneously achieved. In acoustics, it remains challenging to realize reflection elimination based on weak dissipation. In our work, this dilemma is solved by developing a Friedrich-Wintgen quasi-BIC supported by two detuned resonant cavities with trivial intrinsic loss [Fig. 1(c)]. Such a quasi-BIC possesses low radiation loss, allowing the incoming waves at a selected frequency to be completely trapped and survive the low intrinsic loss for a long time. In stark contrast to the previous understanding that a significant amount of intrinsic loss is necessary to guarantee the reflectionless effect, our study demonstrates that a quasi-BIC permits an arbitrarily low intrinsic loss to achieve a zero reflection.

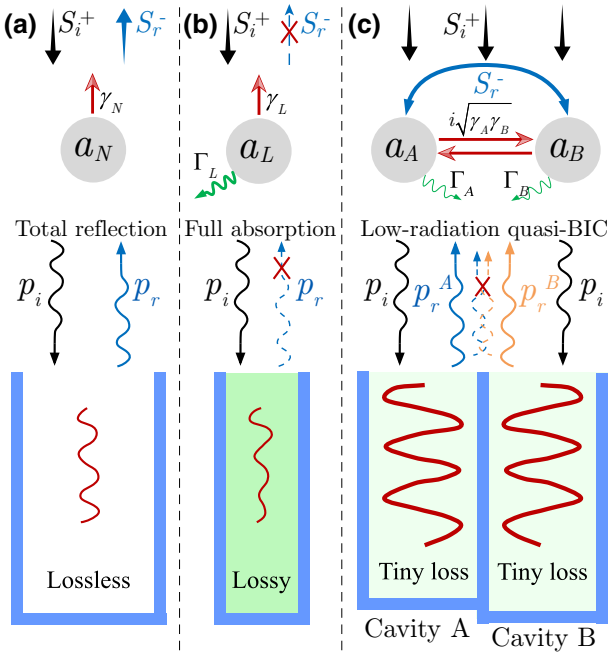

FIG. 1. Sound confinement via a BIC. (a) Unity reflection in a lossless resonant cavity. Blue blocks represent rigid structures. p_i and p_r represent the incident and reflected waves. (b) Zero reflection for a lossy cavity (perfect absorber). (c) Friedrich-Wintgen quasi-BIC-induced wave confinement in two detuned resonators (cavities) with tiny intrinsic losses. $p_r^A(B)$ represents the reflected waves from the Cavity $A(B)$. Upper panels are the schematic illustrations of the corresponding systems below. S_i^+ and S_r^- represent the incident and reflected waves. $a_{N(L)}$ and $\gamma_{N(L)}$ denote the mode amplitude and the radiative decay rate of the lossless (or lossy) system. Γ_L is the dissipative decay rate of the lossy system.

In the practical design, our system consists of two rectangular cavities having the same cross section but different lengths [Fig. 2(a)]. The opening size of the cavities is at the subwavelength scale so that only the fundamental mode exists in the frequency range of interest. Then each cavity (A and B) can be described by the temporal coupled-mode equations for the lowest mode with amplitude (Fig. 1) $\tilde{a}_{A(B)} = a_{A(B)}e^{i\omega t}$ as [44–46],

$$\frac{d}{dt}\tilde{a}_{A(B)} = [i\omega_{A(B)} - \gamma_{A(B)} - \Gamma]\tilde{a}_{A(B)} + i\sqrt{\gamma_{A(B)}}[\tilde{S}_i^+ + i\sqrt{\gamma_{B(A)}}\tilde{a}_{B(A)}], \quad (1)$$

where S_i^+ represents the incident waves, $\omega_{A(B)}$ is the resonant frequency of cavity $A(B)$, $\gamma_{A(B)}$ is the corresponding radiative decay rate, and Γ represents the dissipative decay rate associated with the intrinsic loss of the cavities [Fig. 1(c)]. Cavities A and B share the same Γ because of the same cross section ($\Gamma_A \approx \Gamma_B = \Gamma$). The term $i\sqrt{\gamma_{B(A)}}\tilde{a}_{B(A)}$ represents the reradiation field caused by the resonance $\tilde{a}_{B(A)}$. The reflection coefficient of the system, r, is given as [45,46]

$$r = 1 + 2i\sqrt{\gamma_A}\frac{a_A}{S_i^+} + 2i\sqrt{\gamma_B}\frac{a_B}{S_i^+}. \quad (2)$$

Based on Eqs. (1)–(2), the reflection amplitude diagram [Fig. 2(b)] is illustrated [47] with the varying length of cavity B (l_A is fixed to 180 mm). In this system, interference of radiation takes place according to the coupling term $i\sqrt{\gamma_A\gamma_B}$ [48]. At $\Delta l = 0$ and 435.8 Hz, it shows a vanishing linewidth, which indicates that the Q factor approaches infinite [2,19]. Under this condition and in the absence of Γ, one of the system's eigenfrequencies becomes purely real that corresponds to a BIC [2,47,49].

An ideal BIC is perfectly isolated and has no access to the external radiation channel. In order to achieve confinement of incident sound, a nonzero Δl is introduced to construct a quasi-BIC [22,50,51]. In this case, the purely real eigenfrequency of the system turns to complex with a tiny imaginary part indicated as the system's radiative decay rate, γ_s [47]. When the system's dissipative decay rate (Γ_s) is tuned to the same value as γ_s, the incident acoustic waves can be completely trapped without any backscattering. This condition is equivalent to the so-called critical coupling [52] but here is fulfilled permitting a low radiative and dissipative decay rate in our study. The reflectionless trapping is manifested by Fig. 2(c) (upper panel), in which a zero point appears at the frequency

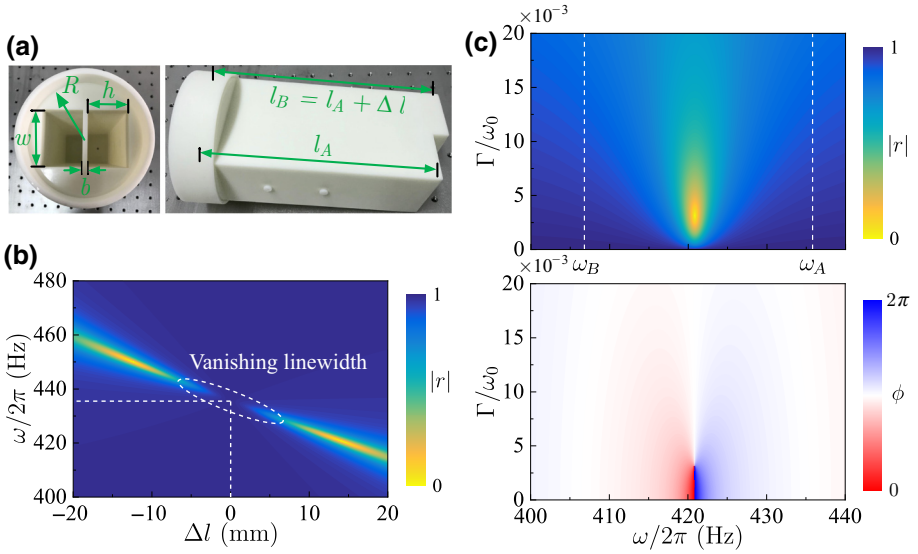

FIG. 2. Acoustic quasi-BIC achieved via two detuned resonant cavities. (a) 3D-printed sample with a width (w) of 38.5 mm and a height (h) of 54 mm. The length of cavity A is fixed to $l_A = 180$ mm. b is the wall thickness, which is set to 4.5 mm. To fit the experimental impedance tube, the two cavities are assembled into a cylindrical adaptor with a radius (R) of 50 mm. (b) Calculated reflection amplitude as a function of the cavities' length difference, Δl, and frequency, $\omega/2\pi$. $\gamma_A = 0.190\omega_A$ and $\gamma_B = 0.191\omega_B$, $\Gamma/\omega_0 = 3.13 \times 10^{-3}$ are extracted from full wave simulations [47]. (c) Calculated reflection amplitude (upper panel) and phase (lower panel) as functions of $\omega/2\pi$ and Γ/ω_0. The length of cavity B is selected as 194 mm. White lines refer to the resonant frequencies of individual cavity A ($\omega_A/2\pi = 435.8$ Hz) and cavity B ($\omega_B/2\pi = 406.8$ Hz).

between ω_A and ω_B ($\omega_0/2\pi = 420.8$ Hz) with a critical low loss of the cavities ($\Gamma/\omega_0 = 3.13 \times 10^{-3}$).

It should be noted that the temporal coupled-mode equations given by Eq. (1) are a generic description of two-mode systems. They are applicable to other structures or wave systems sharing the similar underlying physics with the presented two-cavity design. Hence, the implementation of the quasi-BIC as well as the confinement effect is not limited to the proposed structure here.

c. Experimental demonstration of sound confinement and field enhancement. Experiments were conducted utilizing a Brüel and Kjær impedance tube with a radius of 50 mm [47], as shown in Fig. 3(a). The cross section of the two cavities is designed wide to minimize the intrinsic loss and guarantee a low inherent dissipation of the system [47,53,54]. Then by suitably modulating the lengths of the cavities to construct a quasi-BIC, we can realize complete reflection elimination based on this weak-dissipation condition. As shown in Fig. 3(b), a zero-reflection ($|r| = 0$) point appears at 420.8 Hz despite the tiny loss within the cavities. The reflection curve exhibits a narrow bandwidth, indicating a high Q factor of the system. At the critical frequency of zero reflection, strong pressure amplification (24.5 dB) is also observed.

Due to the fact that the incoming waves are trapped, intensively enhanced field is consequently formed in this presented quasi-BIC-supporting system. To examine the sound-field enhancement, we measure the acoustic pressure amplitudes at two other positions, respectively, arranged near the middle (point 2) and the top (point 3) of cavity A [see Fig. 3(a)]. Results show that the pressure amplitudes at these positions, respectively, reach 22.7 and 19.4 dB of enhancement compared to that of the incident waves [Figs. 3(b)–3(d)]. This reveals that the strong field enhancement nearly occupies the entire cavity A and results in a tremendous energy store, which is distinct from the field enhancement that is induced by wave compression and concentrated in a small area [55,56]. The phenomenon of strong field enhancement in both cavities A and B is further confirmed by the simulated acoustic fields [47]. Moreover, since the quasi-BIC-induced zero reflection is also characterized by a total absorption, acoustic impedance of the system is analyzed [47] and measured to help examine the scattering properties. Due to the relatively large scale of the cavities, the individual cavities are with trivial resistances and exhibit very low absorption peaks [$\alpha_{A(B)} < 0.08$] [the top and bottom figures in Fig. 3(e)]. Nevertheless, as long as three impedance conditions are satisfied, namely $x_A \approx x_B, y_A \approx -y_B$, and $(x_A x_B + |y_A y_B|)/(x_A + x_B) = \rho c$ [47], a matched impedance of the overall structure required by total sound absorption can be achieved [the middle figure in Fig. 3(e)].

d. Transient analysis. In addition to the steady-state analysis above, we perform a transient simulation in the time domain [47] to reveal the wave behavior during the development of the confined sound field. In the simulation,

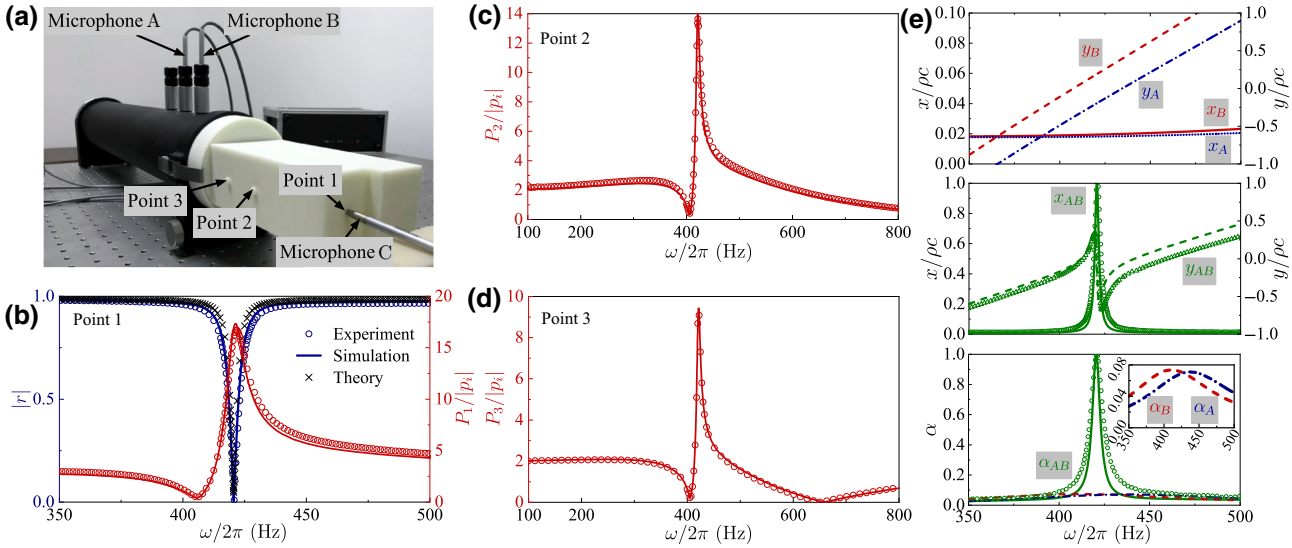

FIG. 3. Experimental demonstration. (a) Experimental setup. Points 1–3 are, respectively, situated at the positions 20, 85, and 130 mm above the inner bottom of cavity A. (b) Reflection factor (blue) and pressure amplification (red) at point 1. Circles, lines, and forks, respectively, represent the experimental, simulated, (frequency domain) and calculated (impedance-based model) results. (c),(d) Pressure amplifications at points 2–3. (e) Impedance measurements and analysis. Top: acoustic impedances of cavities A (blue lines) and B (red lines). $x_{A(B)}$ and $y_{A(B)}$ represent the resistance and resistance of cavity $A(B)$. Middle: acoustic impedance of the overall coherent system. The solid line and circles represent the theoretical and experimental coherent resistance (x_{AB}). The dotted line and triangles represent the theoretical and experimental coherent reactance (y_{AB}). Bottom: absorption coefficients of the coherent system (green), individual cavity A (blue) and B (red).

two points, point 1 (20 mm above the bottom of cavity A) and point 4 (200 mm above the opening, indicated in Fig. S3(a) within the Supplemental Material [47]), are selected to evaluate the acoustic pressure variations inside and outside the BIC-supporting system under continuous incident plane waves of unity amplitude (1 Pa). As the stable interference is established, no acoustic wave is able to escape from the system, in which case the reflected waves cannot reach point 4, and hence the pressure amplitude at point 4 is identical to that of the incident waves. As shown in Fig. 4(a), the instantaneous pressure variation at point 4 experiences several cycles of fluctuations to achieve a stable amplitude of 1 Pa. On the other hand, the pressure amplitude at point 1 gradually increases as the continuous incident waves arrive [Fig. 4(b)], signifying the confinement behavior occurs from the very beginning. Note that the maximum amplitude value is governed by the intrinsic loss of the system [47]. Similar wave behavior is also observed in cavity B [47]. These transient responses clearly display how the incident waves accumulate into a trapped sound field and further validate the extreme sound-confinement effect.

e. Discussion and conclusion. We realize an acoustic Friedrich-Wintgen quasi-BIC with detuned resonant cavities, and experimentally observe the extreme confinement of incident sound together with intensive field enhancement. Compared to those BIC- or quasi-BIC-supporting systems in optics and photonics [2], the relatively large intrinsic loss in acoustic systems, induced by the inevitable thermal and viscous boundary layers inside the structures, hinders an ultrahigh Q factor in experiments. By increasing the opening width of the cavities to reduce the thermal-viscous effect, the Q factor can be improved. For instance, a Q of around 1000 with 50 times of pressure amplification is available when the cavities' openings are broadened to $w = 400$ mm [47]. Theoretically, as can be manifested by the temporal coupled-mode theory [47] and inferred from the impedance analysis [47], the presented sound-confinement system can be developed with arbitrarily low intrinsic loss and possess arbitrarily high Q factor approaching an infinite confinement lifetime.

Our work opens up avenues for the study of the intriguing physics of acoustic BICs, and the qualities observed in such quasi-BIC-supporting systems may facilitate high-performance sensing, ultranarrow band filtering and absorption, and wave and energy harvesting [2,55].

Acknowledgments. This work is supported by the National Natural Science Foundation of China (Grants No. 11704284, No. 11774297, and No. 11774265), and the Young Elite Scientists Sponsorship by CAST (Grant No. 2018QNRC001). S. Huang and T. Liu contributed equally to this work.

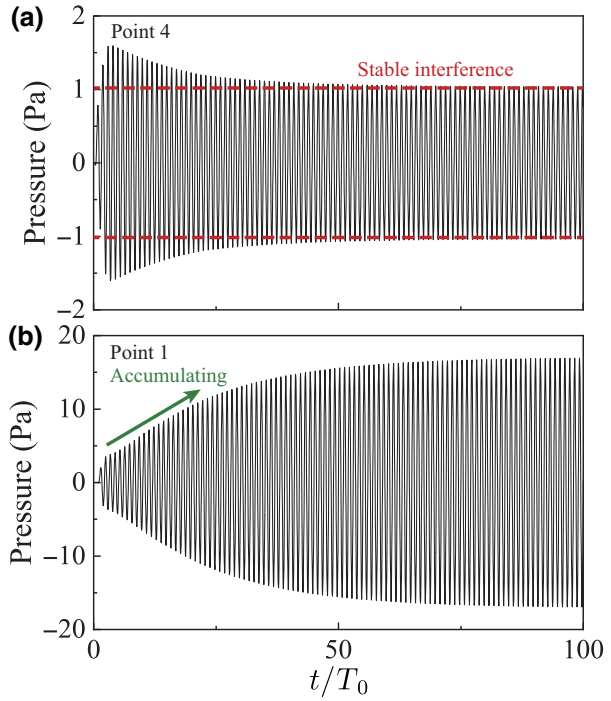

FIG. 4. Time-domain simulation. (a),(b), Time-dependent sound-pressure fluctuations at point 4 and point 1. Point 4 is located at the position 200 mm above the cavity opening [47]. T_0 is the time period of the incident waves.

[1] J. von Neumann and E. Wigner, Über merkwürdige diskrete Eigenwerte, Phys. Z **30**, 465 (1929).

[2] C. W. Hsu, B. Zhen, A. D. Stone, J. D. Joannopoulos, and M. Soljacic, Bound states in the continuum, Nat. Rev. Mater. **1**, 16048 (2016).

[3] R. Parker, Resonance effects in wake shedding from parallel plates: Some experimental observations, J. Sound Vib. **4**, 62 (1966).

[4] S. Hein, W. Koch, and L. Nannen, Trapped modes and fano resonances in two-dimensional acoustical duct-cavity systems, J. Fluid Mech. **692**, 257 (2012).

[5] A. Lyapina, A. Pilipchuk, and A. Sadreev, Trapped modes in a non-axisymmetric cylindrical waveguide, J. Sound Vib. **421**, 48 (2018).

[6] A. A. Lyapina, D. N. Maksimov, A. S. Pilipchuk, and A. F. Sadreev, Bound states in the continuum in open acoustic resonators, J. Fluid Mech. **780**, 370 (2015).

[7] S. Hein and W. Koch, Acoustic resonances and trapped modes in pipes and tunnels, J. Fluid Mech. **605**, 401 (2008).

[8] F. Dreisow, A. Szameit, M. Heinrich, R. Keil, S. Nolte, A. Tunnermann, and S. Longhi, Adiabatic transfer of light via a continuum in optical waveguides, Opt. Lett. **34**, 2405 (2009).

[9] H. M. Doeleman, F. Monticone, W. den Hollander, A. Alu, and A. F. Koenderink, Experimental observation of a polarization vortex at an optical bound state in the continuum, Nat. Photonics **12**, 397 (2018).

[10] Y. Plotnik, O. Peleg, F. Dreisow, M. Heinrich, S. Nolte, A. Szameit, and M. Segev, Experimental Observation of Optical Bound States in the Continuum, Phys. Rev. Lett. **107**, 183901 (2011).

[11] T. Lepetit and B. Kante, Controlling multipolar radiation with symmetries for electromagnetic bound states in the continuum, Phys. Rev. B **90**, 241103 (2014).

[12] D. C. Marinica, A. G. Borisov, and S. V. Shabanov, Bound States in the Continuum in Photonics, Phys. Rev. Lett. **100**, 183902 (2008).

[13] E. N. Bulgakov and A. F. Sadreev, Bound states in the continuum in photonic waveguides inspired by defects, Phys. Rev. B **78**, 075105 (2008).

[14] S. Weimann, Y. Xu, R. Keil, A. E. Miroshnichenko, A. Tunnermann, S. Nolte, A. A. Sukhorukov, A. Szameit, and Y. S. Kivshar, Compact Surface Fano States Embedded in the Continuum of Waveguide Arrays, Phys. Rev. Lett. **111**, 240403 (2013).

[15] C. W. Hsu, B. Zhen, J. Lee, S. L. Chua, S. G. Johnson, J. D. Joannopoulos, and M. Soljacic, Observation of trapped light within the radiation continuum, Nature **499**, 188 (2013).

[16] F. Monticone and A. Alu, Embedded Photonic Eigenvalues in 3d Nanostructures, Phys. Rev. Lett. **112**, 213903 (2014).

[17] M. I. Molina, A. E. Miroshnichenko, and Y. S. Kivshar, Surface Bound States in the Continuum, Phys. Rev. Lett. **108**, 070401 (2012).

[18] S. I. Azzam, V. M. Shalaev, A. Boltasseva, and A. V. Kildishev, Formation of Bound States in the Continuum in Hybrid Plasmonic-Photonic Systems, Phys. Rev. Lett. **121**, 253901 (2018).

[19] A. Kodigala, T. Lepetit, Q. Gu, B. Bahari, Y. Fainman, and B. Kante, Lasing action from photonic bound states in continuum, Nature **541**, 196 (2017).

[20] C. Huang, C. Zhang, S. Xiao, Y. Wang, Y. Fan, Y. Liu, N. Zhang, G. Qu, H. Ji, and J. Han, *et al.*, Ultrafast control of vortex microlasers, Science **367**, 1018 (2020).

[21] B. Midya and V. V. Konotop, Coherent-perfect-absorber and laser for bound states in a continuum, Opt. Lett. **43**, 607 (2018).

[22] L. Cong and R. Singh, Symmetry-protected dual bound states in the continuum in metamaterials, Adv. Opt. Mater. **7**, 1900383 (2019).

[23] A. A. Yanik, A. E. Cetin, M. Huang, A. Artar, S. H. Mousavi, A. Khanikaev, J. H. Connor, G. Shvets, and H. Altug, Seeing protein monolayers with naked eye through plasmonic fano resonances, P. Natl. Acad. Sci. USA **108**, 11784 (2011).

[24] S. Romano, G. Zito, S. N. L. Yépez, S. Cabrini, E. Penzo, G. Coppola, I. Rendina, and V. Mocellaark, Tuning the exponential sensitivity of a bound-state-in-continuum optical sensor, Opt. Express **27**, 18776 (2019).

[25] J. M. Foley, S. M. Young, and J. D. Phillips, Symmetry-protected mode coupling near normal incidence for narrow-band transmission filtering in a dielectric grating, Phys. Rev. B **89**, 165111 (2014).

[26] L. L. Doskolovich, E. A. Bezus, and D. A. Bykov, Integrated flat-top reflection filters operating near bound states in the continuum, Photonics Res. **7**, 1314 (2019).

[27] R. Parker and W. M. Griffiths, Low frequency resonance effects in wake shedding from parallel plates, J. Sound Vib. **7**, 371 (1968).
[28] R. Parker, Resonance effects in wake shedding from parallel plates: Calculation of resonant frequencies, J. Sound Vib. **5**, 330 (1967).
[29] N. A. Cumpsty and D. Whitehead, The excitation of acoustic resonances by vortex shedding, J. Sound Vib. **18**, 353 (1971).
[30] W. Koch, Resonant acoustic frequencies of flat plate cascades, J. Sound Vib. **88**, 233 (1983).
[31] R. Parker and S. Stoneman, The excitation and consequences of acoustic resonances in enclosed fluid flow around solid bodies, P. I. Mech. Eng. C-J. Mec. **203**, 9 (1989).
[32] D. Evans, M. Levitin, and D. Vassiliev, Existence theorems for trapped modes, J. Fluid Mech. **261**, 21 (1994).
[33] D. Evans, C. Linton, and F. Ursell, Trapped mode frequencies embedded in the continuous spectrum, Q. J. Mech. Appl. Math. **46**, 253 (1993).
[34] M. Groves, Examples of embedded eigenvalues for problems in acoustic waveguides, Math. Method. Appl. Sci. **21**, 479 (1998).
[35] C. Linton and M. McIver, Trapped modes in cylindrical waveguides, Q. J. Mech. Appl. Math. **51**, 389 (1998).
[36] J. Mei, G. Ma, M. Yang, Z. Yang, W. Wen, and P. Sheng, Dark acoustic metamaterials as super absorbers for low-frequency sound, Nat. Commun. **3**, 756 (2012).
[37] G. Ma, M. Yang, S. Xiao, Z. Yang, and P. Sheng, Acoustic metasurface with hybrid resonances, Nat. Mater. **13**, 873 (2014).
[38] Y. Li and B. M. Assouar, Acoustic metasurface-based perfect absorber with deep subwavelength thickness, Appl. Phys. Lett. **108**, 063502 (2016).
[39] S. B. Huang, X. S. Fang, X. Wang, B. Assouar, Q. Cheng, and Y. Li, Acoustic perfect absorbers via helmholtz resonators with embedded apertures, J. Acoust. Soc. Am. **143**, 254 (2019).
[40] S. B. Huang, X. S. Fang, X. Wang, B. Assouar, Q. Cheng, and Y. Li, Acoustic perfect absorbers via spiral metasurfaces with embedded apertures, Appl. Phys. Lett. **113**, 233501 (2018).
[41] J. Li, W. Wang, Y. Xie, B.-I. Popa, and S. A. Cummer, A sound absorbing metasurface with coupled resonators, Appl. Phys. Lett. **109**, 12 (2016).
[42] C. Zhang and X. Hu, Three-Dimensional Single-Port Labyrinthine Acoustic Metamaterial: Perfect Absorption with Large Bandwidth and Tunability, Phys. Rev. Appl. **6**, 064025 (2016).
[43] S. Huang, Z. Zhou, D. Li, T. Liu, X. Wang, J. Zhu, and Y. Li, Compact broadband acoustic sink with coherently coupled weak resonances, Sci. Bull. **65**, 373 (2020).
[44] S. H. Fan, W. Suh, and J. D. Joannopoulos, Temporal coupled-mode theory for the fano resonance in optical resonators, J. Opt. Soc. Am. A **20**, 569 (2003).
[45] W. W. Zhu, X. S. Fang, D. T. Li, Y. Sun, Y. Li, Y. Jing, and H. Chen, Simultaneous Observation of a Topological Edge State and Exceptional Point in an Open and Non-Hermitian Acoustic System, Phys. Rev. Lett. **121**, 124501 (2018).
[46] W. Tan, Y. Sun, Z. G. Wang, and H. Chen, Manipulating electromagnetic responses of metal wires at the deep subwavelength scale via both near- and far-field couplings, Appl. Phys. Lett. **104**, 091107 (2014).
[47] See Supplemental Material at http://link.aps.org/supplemental/10.1103/PhysRevApplied.14.021001 for details on the eigenvalues analysis, the experimental setup, the simulation results, the impedance analysis, etc.
[48] H. Friedrich and D. Wintgen, Interfering resonances and bound states in the continuum, Phys. Rev. A **32**, 3231 (1985).
[49] M.-A. Miri and A. Alù, Exceptional points in optics and photonics, Science **363**, eaar7709 (2019).
[50] Z. Liu, Y. Xu, Y. Lin, J. Xiang, T. Feng, Q. Cao, J. Li, S. Lan, and J. Liu, High-Q Quasibound States in the Continuum for Nonlinear Metasurfaces, Phys. Rev. Lett. **123**, 253901 (2019).
[51] K. Koshelev, S. Lepeshov, M. Liu, A. Bogdanov, and Y. Kivshar, Asymmetric Metasurfaces with high-Q Resonances Governed by Bound States in the Continuum, Phys. Rev. Lett. **121**, 193903 (2018).
[52] K. Y. Bliokh, Y. P. Bliokh, V. Freilikher, S. Savel'ev, and F. Nori, Colloquium: Unusual resonators: Plasmonics, metamaterials, and random media, Rev. Mod. Phys. **80**, 1201 (2008).
[53] U. Ingard, On the theory and design of acoustic resonators, J. Acoust. Soc. Am. **25**, 1037 (1953).
[54] M. R. Stinson, The propagation of plane sound waves in narrow and wide circular tubes, and generalization to uniform tubes of arbitrary cross–sectional shape, J. Acoust. Soc. Am. **89**, 550 (1991).
[55] Y. Y. Chen, H. J. Liu, M. Reilly, H. Bae, and M. A. Yu, Enhanced acoustic sensing through wave compression and pressure amplification in anisotropic metamaterials, Nat. Commun. **5**, 5247 (2014).
[56] J. Zhu, Y. Chen, X. Zhu, F. J. Garcia-Vidal, X. Yin, W. Zhang, and X. Zhang, Acoustic rainbow trapping, Sci. Rep. **3**, 1728 (2013).